Science of the Total Environment 838 (2022) 156436

Contents lists available at ScienceDirect

Science of the Total Environment

journal homepage: www.elsevier.com/locate/scitotenv

The effects of weathering of coal-bearing stratum on the transport and transformation of DIC in karst watershed

Jiangxun Huang [a], Qingguang Li [a,*], Pan Wu [a], Shilu Wang [b], Mingwei Guo [b], Kun Liu [b]

[a] College of Resources and Environmental Engineering, Key Laboratory of Karst Georesources and Environment, Ministry of Education, Guizhou University, Guiyang 550025, China
[b] State Key Laboratory of Environmental Geochemistry, Institute of Geochemistry, Chinese Academy of Sciences, Guiyang 550081, China

HIGHLIGHTS

- The differential weathering-leaching of sulfide-rich coal-measures in different seasons induces a lower water pH in the rainy season and a higher pH in the dry season.
- DIC transformation is controlled by AMD input, CO2 degassing, OM degradation, and carbonates dissolution and precipitation in different seasons.
- Due to the mass input of AMD, the river shows to drive CO2 outgassing in autumn.

GRAPHICAL ABSTRACT

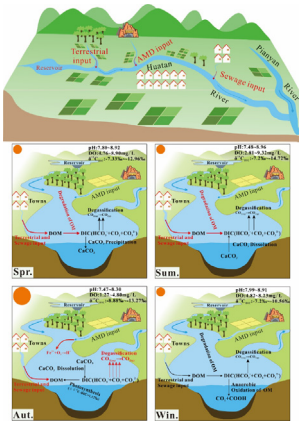

ARTICLE INFO

Editor: José Virgílio Cruz

Keywords:
DIC transport and transformation
CO_2 outgassing
Buffering capacity
Sulfide-rich coal measures
Seasonal variations

ABSTRACT

The mining of medium- to high-sulfur coal in karst areas has led to serious acidification problems in surface water, thus encouraging a re-evaluation of DIC transformation and CO_2 source-sink relationships in karst watersheds. The weathering of limestone and sulfide-rich coal measures jointly influence the pH of the Huatan River in karst areas in Southwest China, which is lower in the rainy season and higher in the dry season. Due to CO_2 degassing, DIC concentration tends to decrease along the flow direction, while δ^{13}C-DIC gradually becomes heavier. In general, DIC transformation in the Huatan River is controlled by AMD input, CO_2 degassing, organic matter (OM) degradation, and the dissolution and precipitation balance of carbonate minerals in different seasons. In spring, the mineralization of OM from terrestrial and domestic sewage gradually enhances and replenishes DIC in the water. As the pH increases in this season, the capacity for buffering CO_2 increases. Meanwhile, OM degradation generates a large amount of CO_2 in summer, and carbonic acid begins to dissolve limestone. In autumn, the pH decreases due to the enhanced weathering of sulfide-rich coal measures and the mass input of AMD. Thus, the river shows the ability to drive CO_2 outgassing. In winter, CO_2 degassing gradually weakens, DIC concentration is at its lowest, and δ^{13}C-DIC reaches the heaviest value.

1. Introduction

Globally, the karst process-related carbon sink is about 0.11–0.80PgC/a (Liu et al., 2010; Liu et al., 2018). In comparison to other countries around the globe, China has the largest karst area in the world, with a karst area of 3.44 million km^2; moreover, karst is widely developed in

* Corresponding author at: College of Resource and Environmental Engineering, Guizhou University, South Huaxi Road, Guiyang 550025, China.
E-mail addresses: 2431033709@qq.com (J. Huang), leegq12@163.com (Q. Li), pwu@gzu.edu.cn (P. Wu), wangshilu@vip.skleg.cn (S. Wang), 1599188103@qq.com (M. Guo), liukun@mail.gyig.ac.cn (K. Liu).

http://dx.doi.org/10.1016/j.scitotenv.2022.156436
Received 23 April 2022; Received in revised form 18 May 2022; Accepted 30 May 2022
Available online 3 June 2022
0048-9697/© 2022 Published by Elsevier B.V.

Southwest China. The weathering of carbonate rocks is an essential CO_2 sink (Wang et al., 2019, 2020; Beaulieu et al., 2012); specifically, this portion of carbon is stored in the form of DIC in the surface water system in the karst area.

In the carbonate strata distribution area of China, coal measures are generally well developed. The mining of medium- to high-sulfur coal has caused serious surface water acidification, in turn complicating the evolution of DIC in surface watersheds. In fact, it is difficult to measure the amount of sulfuric acid-driven carbonate dissolution (Singer and Stumm, 1970; Eq. (1)). The acid production from the hydrolysis of metal ions such as Fe^{3+} is considerable during pyrite oxidation, and the oxidation of reduced Fe^{2+} can cause an unsaturation of dissolved oxygen (DO) in the water. In this case, the anaerobic oxidation of dissolved organic carbon (DOC) will produce a certain amount of organic acid, leading to a further increase in the dissolution of carbonate rock. It can be seen that DIC evolution in a surface watershed is controlled by more than karstification-related processes in areas where carbonate rocks and medium- to high-sulfur coal measures coexist. Therefore, a systematic study of the source, transport, and transformation of DIC within surface water systems driven by acid mine drainage (AMD) can help to further characterize the DIC evolution and CO_2 source-sink relationships in karst watersheds.

$$FeS_2 + 14Fe^{3+} + 8H_2O = 15Fe^{2+} + 2SO4^{2-} + 16H^+ \quad (1)$$

Typically, the evolution of DIC in surface water is primarily driven by CO_2 outgassing, weathering of silicate and carbonate rocks, precipitation and dissolution of calcite, the degradation of OM, and so on (Wang et al., 2011; Weyhenmeyer et al., 2015; Lu et al., 2018). As the intensity of human activities continues to increase, the mineralization of soil OM and the input of domestic sewage also contribute large amounts of DIC to surface water. As carbonate rocks undergo weathering, if the CO_2 has resulted from the mineralization of soil OM, $\delta^{13}C$ of the generated DIC should reflect the carbon isotopic composition of carbonate rocks and soil OM (Zhang et al., 2014; Liu and Han, 2020). Even though the $\delta^{13}C$ of DIC produced by H^+ erosion of limestone should mainly inherit the signal of carbonate rock (Zhang et al., 1995; Song et al., 2021; ~0 ‰), a series of other processes in surface waters are known to affect the evolution of DIC. For example, aquatic photosynthesis converts DIC into DOC, a process that raises the pH of the water and promotes the precipitation of calcium carbonate (Chen et al., 2021; Zhong et al., 2021; Wang et al., 2015; Eq. (2)). CO_2 outgassing also causes isotopic fractionation between different DIC components (Wang et al., 2019, 2020; Liu and Zhao, 2000; Gombert, 2002). Fonyuy and Atekwana (2008a) found that, being affected by the input of AMD, CO_2 degassing in a surface watershed led to heavier $\delta^{13}C$-DIC by 1.0 ‰ ~ 3.0 ‰, and 50 % ~ 98 % of the DIC was released into the atmosphere through CO_2 outgassing. In addition, the carbonate components may have a certain buffer effect on the acidity of water and restrain CO_2 outgassing (Zhang et al., 2019).

$$67Ca^{2+} + 134HCO_3^- + 39CO_2 + 16HNO_3 + H_3PO_4 + 55H_2O \rightarrow (CH_2O)_{106}(NH_3)_{16}(H_3PO_4) + 67CaCO_3 + 138O_2 \quad (2)$$

Guizhou is characterized by a typical karst landscape, with carbonate rocks covering 73 % of the land area of the entire province (Han and Liu, 2004). Additionally, Guizhou also has abundant coal resources, with a coal output of 145 million tons in 2020. Most of this coal is medium- to high-sulfur coal. However, the impact of AMD on DIC in surface water systems during coal development has received insufficient attention (Mayo et al., 2000; Fonyuy and Atekwana, 2008b). Accordingly, the Huatan River, having this type of geological background, was selected as the study object. Analyses of pH, DIC concentration, $\delta^{13}C$-DIC, and the Revelle factor were conducted to reveal the temporal and spatial evolution characteristics of DIC and $\delta^{13}C$-DIC under the influence of AMD input. The following discussion of the main controlling factors affecting the evolution of DIC is intended to deepen the understanding of the carbon transport process of a surface water system in a karst area.

2. Overview of the study area

The Huatan River Basin is located in the eastern part of Jinsha County, Guizhou Province (E: 106°26′ ~ 106°42′, N: 27°16′ ~ 27°28′). The basin covers an area of 321 km^2, with a total length of 59 km, a natural drop of 220 m, and an average annual runoff of 130 million m^3. This region can be described as having a subtropical monsoon humid climate, with a mild climate and annual average rainfall of 1057 mm. The groundwater level changes significantly with the season. Water levels begin to rise in May every year, and the highest water level is from June to September, while the normal water period is from October to December, and the lowest is in March and April of the next year.

There is a reservoir at the upstream of the river, with a storage capacity of 6.75 million m^3. After entering the Shatu Town, several tributaries add their inflow successively. Among them, the Chetian River, a vital tributary on the left bank, is 12.6 km long, with a drainage area of 23.93 km^2. Along this tributary are found Huixin, Hongxing, Yutiancheng, and other coal mines. A large amount of AMD is produced by coal mining, causing the river's pH to reach levels as low as 3.05 and thereby exerting a significant impact on the Huatan River.

The Huatan River Basin is located in the North-East tectonic deformation zone of the north Guizhou platform uplift in the Yangtze platform. The main structural features are the North-Eastern trending folds and faults. The strata exposed in the basin include the Cambrian Loushanguan Formation ($\epsilon_{2\text{-}3}ls_2$), the Lower Permian Maokou Formation (P_1m), the Upper Permian Longtan Formation (P_2l), the Changxing Formation (P_2c), the Lower Triassic Yelang Formation (T_1y_1), the Yulongshan Section (T_1y_2), the Maocaopu Formation (T_1m_1), the Shizishan Formation (T_2sh), the Songzikan Formation (T_2s), and the loose Quaternary sediments (Q).

In terms of lithology, the area mainly contains carbonate rocks and clastic rocks. Carbonate rocks are widely distributed. Funnels, crests, depressions, ponors, volcanoes, and natural bridges can be seen everywhere. The Longtan Formation is a coal-bearing rock system, about 95–110 m in thickness and containing a total of 4–8 coal layers. In particular, the pyrite ore sections occurring at the bottom of the Longtan Formation and above the Maokou Formation are patchy, nodular, and scattered, being unevenly distributed in clay rocks. Industrial ore bodies are formed in certain sections, with a thickness of 0.8–1.8 m.

3. Sample collection and analysis

3.1. Sample collection

In this study, 18 sampling sites were set up along the river flow (Fig. 1). The sampling campaign was conducted from November 2020 to November 2021. A total of 234 water samples were collected during the 13-month sampling period. A YSI Pro Plus multi-parameter water quality analyzer was used to determine temperature, pH, dissolved oxygen (DO), and other variable parameters. The electrodes were calibrated the night before sampling according to the manufacturer's specifications. The alkalinity was titrated on-site using the Merck titration box (Item No. 1.11109.0001). This parameter required three parallel samples to be titrated continuously to ensure that the error was within 0.05 mmol. The concentrations of DIC and different DIC components are calculated based on the chemical equilibrium of $H_2CO_3 - HCO_3^- - CO_3^{2-}$, pH, and alkalinity but does not account for the uncertainties of water temperature and EC. The specific calculation method was developed by Liu and Han (2020) and Rosentreter and Eyre (2020). The water samples were filtered on-site with 0.45 μm filter membrane under positive pressure. For cation analysis, the aliquot was added with nitric acid to adjust the pH < 2.0. Meanwhile, for anion analysis, no reagent was added, and for $\delta^{13}C$-DIC analysis, the samples were filtered through 0.45 μm nylon membrane with positive pressure and stored bubble-free in 50 mL brown glass bottles. All samples were maintained at 4 °C until analysis.

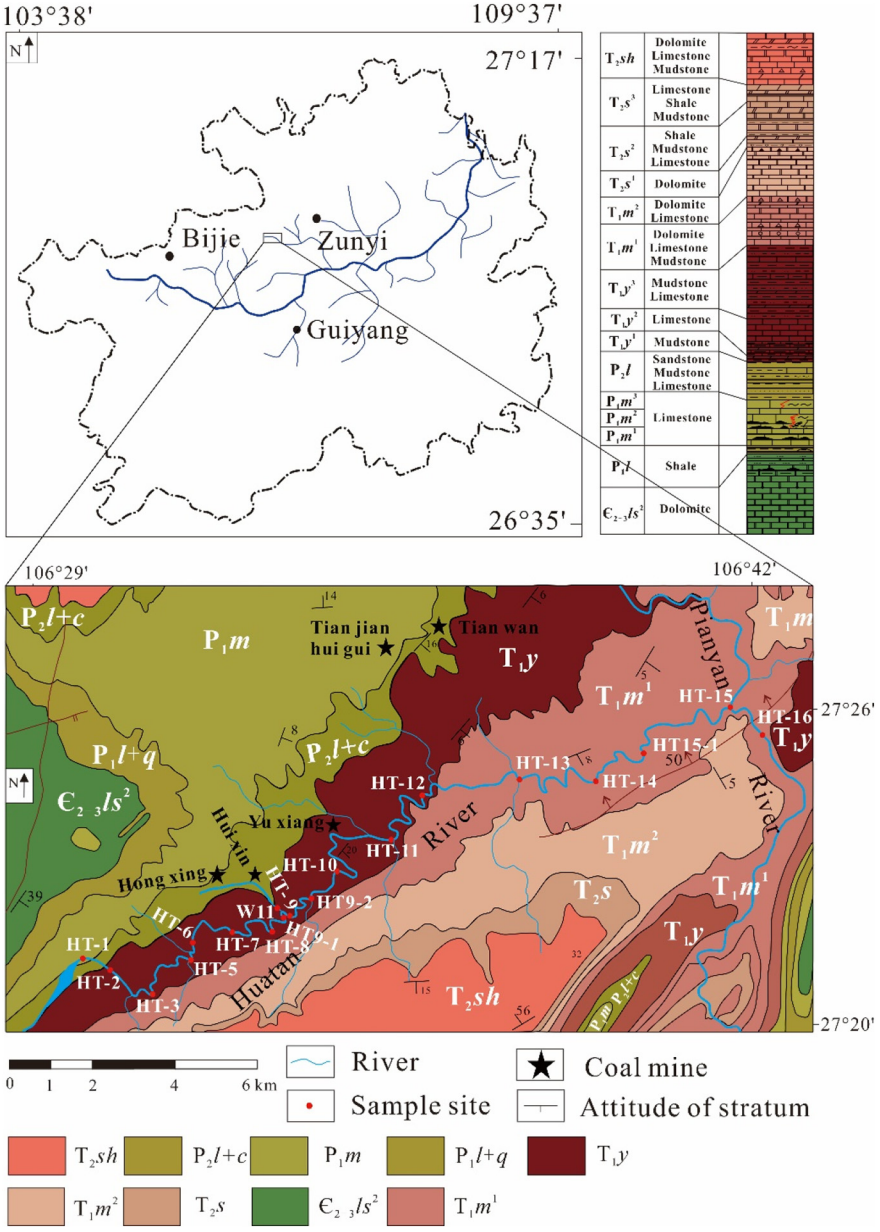

Fig. 1. Sampling point map of the Huatan River Basin.

3.2. Analysis

SO_4^{2-}, Cl^-, NO_3^-, and F^- were analyzed with an ICS-90 ion chromatograph produced by Dionex, Inc., USA. The concentration of Ca^{2+}, Mg^{2+}, Na^+, and K^+ were determined by a Vista MPX inductively coupled plasma optical emission spectrometer (ICP-OES) produced by Varian, Inc., USA. Blank samples and parallel samples were added for quality control. The charge balance error was controlled within 5 %. The anion and anion tests were conducted in the State Key Laboratory of Environmental Geochemistry, Institute of Geochemistry, Chinese Academy of Sciences.

A Delta V Advantage gas isotope mass spectrometer equipped with a Gasbench was used to analyze the δ^{13}C-DIC. First, 0.2 mL of high-purity phosphoric acid was added to a high-borosilicate glass vial. Then, high-purity He was used to purge the glass vial for approximately 7 min. Subsequently, a 0.5 mL water sample was injected into the glass vial and equilibrated for 1 h. The generated CO_2 was loaded into the mass spectrometer via He for isotopic analysis. Interspersed parallel samples and international standard samples NBS18 and IAEA603 were used for quality control. The measured carbon isotopes were expressed as δ^{13}C-DIC (‰) using the international standard sample VPDB, and the calculation equation was as follows:

$$\delta^{13}C_{DIC}(‰) = \left[\left(R_{Sample}/R_{VPDB}\right) - 1\right] \times 1000‰ \quad (3)$$

$$\delta^{13}C_{CO_2} = \delta^{13}C_{DIC} + 23.644 - \frac{9701.5}{T} \quad (4)$$

$$\Delta_{HCO_3^- - CO_2} = -9.866 \times \frac{10^3}{T} + 24.12 = \delta^{13}C_{HCO_3^-} - \delta^{13}C_{CO_2} \quad (5)$$

3.3. Calculation of buffer factor

Due to the existence of a self-delivering equilibrium process among carbonate components, surface water has a certain buffering capacity in terms of absorbed CO_2 (Eq. (6); Broecker et al., 1979; Revelle and Suess, 1957). This capacity can be calculated using Eq. (7), in which TCO_2 denotes total

dissolved inorganic carbon (Egleston et al., 2010; Zhang et al., 2019). The larger the Revelle factor, the lower the buffering capacity of the water will be for CO_2.

$$CO_2 + CO_3^{2-} + H_2O = 2HCO_3^- \quad (6)$$

$$R = TCO_2/([CO_2] + [CO_3^{2-}]) \quad (7)$$

4. Results

4.1. Conventional water chemistry parameters

The pH in the Huatan River Basin was lower in summer and autumn (7.47–8.96, 8.06 on average) and higher in winter and spring (7.80–8.92, 8.43 on average). The pH of rainwater collected in summer was 5.64.

The temperature in summer ranged from 18.6 to 30.4 °C, with an average water temperature of 23.2 °C. In contrast, winter temperatures ranged from 6.2 to 18.8 °C, with an average water temperature of 12.5 °C. In terms of spatial distribution, the water flow and water depth gradually increased during the runoff process, and the water temperature had a tendency to increase gradually with distance traveled.

DO in the Huatan River Basin ranged from 1.27 to 9.32 mg/L throughout the year, with an average of 5.22 mg/L. Overall, DO demonstrated obvious seasonal changes, being high in winter and spring versus low in summer and autumn. Considering that the pH was lower in summer and autumn than in winter and spring, the oxidation of reducing metal ions leached out of the coal-bearing rock systems may be a noteworthy factor influencing the seasonal variation of DO.

4.2. DIC concentration and carbon isotopes

As can be seen from Fig. 2, the DIC concentration showed a clear seasonal variation, high in autumn (2.84 to 4.53 mmol/L, 3.92 mmol/L on average) and low in winter (2.84 to 4.53 mmol/L, 3.16 mmol/L on average). Spatially, the overall trend of DIC concentration decreased from upstream to downstream. In October 2021, a 60 % loss of DIC was observed from HT1 to HT16. In particular, HT5 and HT9 showed a significant

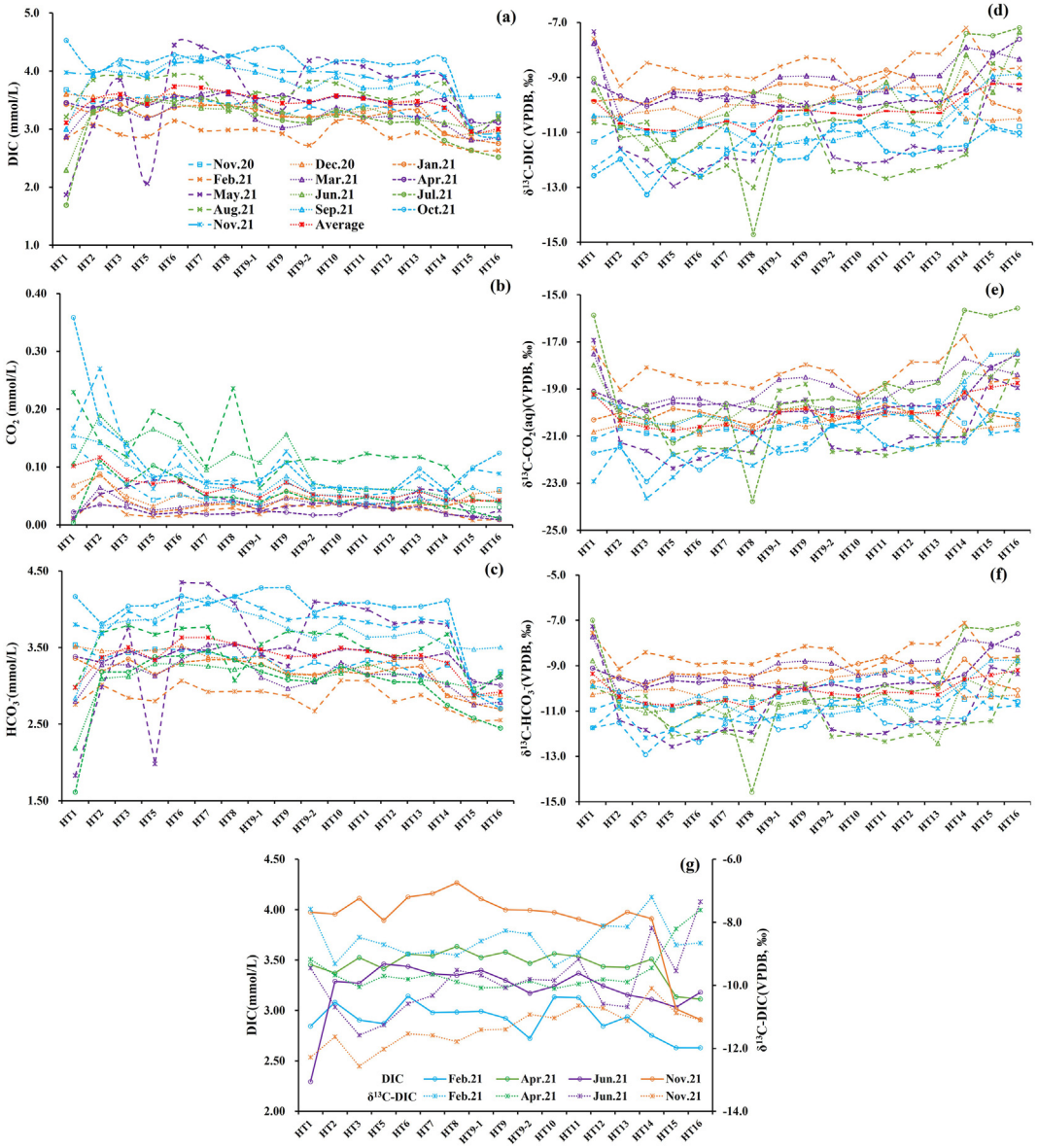

Fig. 2. (a)-(c) Spatial and temporal variation of DIC, CO_2, and HCO_3^- concentrations; (d)-(f) Spatial and temporal variation of δ^{13}C-DIC, δ^{13}C-CO_2 and δ^{13}C-HCO_3^- in the Huatan River Basin; (g) Co-evolution of DIC and δ^{13}C-DIC in different seasons.

decrease in DIC concentrations due to the input of two AMD-influenced tributaries at these two points. From Fig. 2, it can be seen that the components of $H_2CO_3^*$ and HCO_3^- show a variation pattern more or less consistent with that of DIC. However, the seasonal variation pattern was more obvious for $H_2CO_3^*$ than DIC.

The δ^{13}C-DIC in the Huatan River also showed an obvious seasonal variation pattern. In autumn, the range of δ^{13}C-DIC was −13.3 ‰ to −8.9 ‰, with an average of −11.2 ‰; In winter, it ranged from −10.6 ‰ to −7.2 ‰, with an average of −9.4 ‰. Interestingly, the DIC concentration and δ^{13}C-DIC exhibited opposite evolutionary trends in different seasons. In summer and autumn, DIC concentration was high, while δ^{13}C-DIC was low (Fig. 2). Contrariwise, in winter and spring, DIC concentration was low, while δ^{13}C-DIC was high. The isotopic variation characteristics among different components of DIC were further revealed by calculating the carbon isotopic compositions of HCO_3^-, CO_2, and CO_3^{2-} for all samples according to Eqs. (4) and (5) (Mook et al., 1974; Samanta et al., 2015; Wang et al., 2019, 2020). The results showed that δ^{13}C-HCO_3^- and δ^{13}C-CO_2 could better reflect the isotopic variation characteristics than δ^{13}C-DIC (Fig. 2).

4.3. Revelle factor

The Revelle factor in the Huatan River ranged from 12.47 to 53.63 throughout the year, with an average of 42.20. In general, the Revelle factor also demonstrated an obvious seasonal variation. As can be seen from Fig. 3, the variation of the Revelle factor along the flow direction resembled the "M" type. It decreased in all seasons at the sampling site HT9, which could be attributed to the input of an AMD-influenced tributary at this site. At the source (HT1) and downstream sampling sites (HT15, HT16), the water was relatively deep. Hence, the influence of aquatic ecological process on the Revelle factor increased. At the remaining sampling sites, the Revelle factor displayed high values, reflecting the carbonate weathering background.

5. Discussion

5.1. The buffering capacity of the carbonate system

In their investigation of the role of carbonate buffering in controlling CO_2 escape, Duvert et al. (2019) found that in rivers with particularly high CO_2 escape, the carbonate system was able to maintain high CO_2 concentrations by adjusting the carbonate balance. Meanwhile, Hauck and Völker (2015) studied CO_2 transport relationships at the South Pacific water-air interface through an analysis of the Revelle factor. The results indicated that the contribution of biological activities to CO_2 uptake has become increasingly important. However, this buffer capacity is not unlimited; there is a limited level in terms of the transformation of different DIC components.

It is generally accepted that the Revelle factor in the ocean averages about 10, while the variability of karst watershed systems ranges from 8 to 50 (Egleston et al., 2010; Zhang et al., 2019; Wang and Li, 2021). Compared with pure carbonate systems and the ocean, the Huatan River, under karstic geological background conditions, had a weaker buffering capacity for CO_2. The illustration in Figs. 3 and 4 reveals that the Revelle factor reached its maximum when pH = 8.46. Similarly, when the TCO_2:alkalinity ratio = 1, CO_3^{2-} = 0.029 mmol/L, and CO_2 = 0.031 mmol/L, according to the Revelle factor, the river had the lowest buffering capacity for carbonate.

This limit value was also observed to occur in winter. At this time, the Huatan River Basin was in the dry season (December 2020 to February 2021). As the rainwater recharged and AMD input was reduced, the pH of the river water gradually increased (pH > 8.46). Next, the proportion of CO_3^{2-} gradually increased, and the Revelle factor gradually decreased. Therefore, this outcome implies an enhancement of atmospheric CO_2 absorption capacity in spring (Fig. 3).

Summer represented the rainy season (June 2021 to August 2021) in the study area. Atmospheric precipitation tended to enhance the leaching of sulfide-rich coal measures. Moreover, coal mining produced a larger

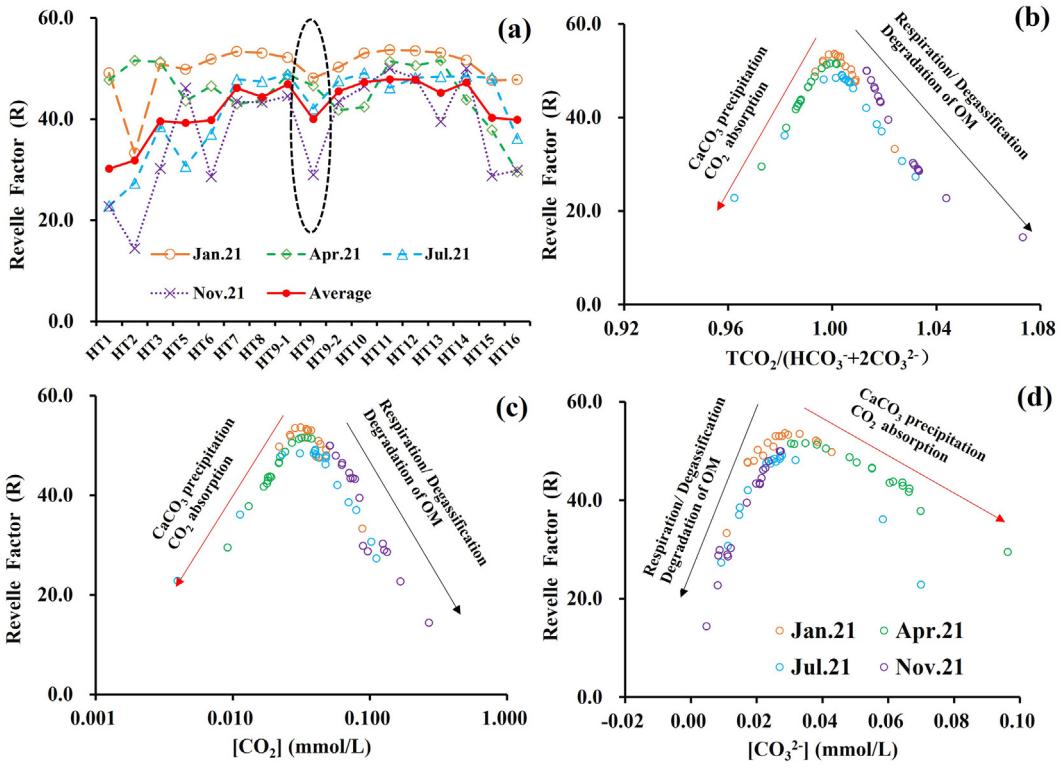

Fig. 3. (a) Spatial and temporal variation of the Revelle Factor; (b) relationship between Revelle Factor and $TCO_2/(HCO_3^- + 2CO_3^{2-})$ ratio; (c) relationship between Revelle Factor and CO_2; and (d) relationship between Revelle Factor and CO_3^{2-} in the Huatan River Basin.

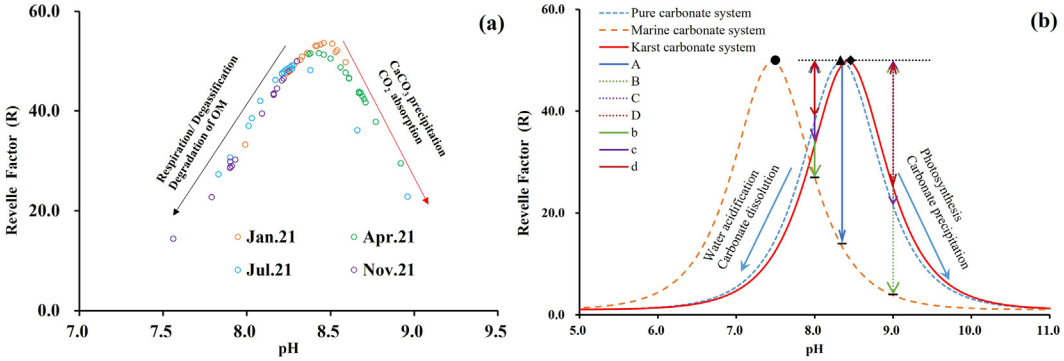

Fig. 4. Relationship between Revelle Factor and pH in the Huatan River Basin and Plot of Revelle Factor versus pH correlation under different aqueous media conditions (A: CO_2 uptake buffering capacity of marine system at pH = 8.38, the weakest pure carbonate buffering capacity; B:CO_2 uptake buffering capacity of marine system at pH = 9.00; C:CO_2 uptake buffering capacity of pure carbonate system at pH = 9.00; D:CO_2 uptake buffering capacity of karst at pH = 9.00; b:CO_2 absorption buffering capacity of the marine system at pH = 8.00; c:CO_2 absorption buffering capacity of the karst system at pH = 8.00; d:CO_2 absorption buffering capacity of the pure carbonate system at pH = 9.00; solid circles (pH = 7.50) are the weakest buffering capacity of the marine system; solid triangles (pH = 8.38) represents the weakest buffering capacity of the pure carbonate system; solid diamond (pH = 8.46) is the weakest buffering capacity in the Huatan River Basin).

amount of AMD (Teemu et al., 2018; Elghali et al., 2018). The river water pH gradually decreased (pH < 8.46), and the Revelle factor decreased. This process was accompanied by strong CO_2 outgassing. Correspondingly, this observation also shows the enhancement of the erosion ability of carbonate rocks.

5.2. The transport and transformation of DIC in the Huatan River

5.2.1. Δ[CO_2] and ΔDO stoichiometric balance

A dynamic equilibrium relationship exists between DO and water-soluble CO_2 in freshwater systems (Wang et al., 2015; Richey et al., 1988). We used ΔCO_2 to define the difference between the actual amount of water-soluble CO_2 and the theoretical value when CO_2 at the water-gas interface reached equilibrium (Richey et al., 1988; Zhai et al., 2005; Eq. (8)); similarly, the apparent oxygen utilization (ΔDO) refers to the difference between the measured DO concentration and the saturated oxygen content under water-gas equilibrium conditions (Richey et al., 1988; Zhai et al., 2005; Eq. (9)).

$$\Delta CO_2 = [CO_2] - K_h \times pCO_2(\text{in } pt\text{air}) \tag{8}$$

$$\Delta DO = \left(DO_{(cal.)} - DO\right)/32 \tag{9}$$

$$DO_{(cal.)} = \frac{(P/P_0) \times 477.8}{T + 32.26} \tag{10}$$

where $[CO_2]$ represents the total free CO_2 in the water; K_h is the equilibrium constant of CO_2; DO is the measured value of dissolved oxygen; P represents the atmospheric pressure in the sampling site in the Huatan River Basin; P_0 represents the standard atmospheric pressure, taking the value of 101 kPa; and T is the measured water temperature (Zhang, 1999).

According to the Redfield equation (Eq. (11)), the ratio of excess CO_2 and apparent oxygen utilization (ΔCO_2:ΔDO) should be 0.90 (Redfield et al., 1963). However, the effect of lipids was not considered in this equation (Chen et al., 1996). Chen et al. (1996) and Hedges et al. (2002) pointed out that ΔCO_2:ΔO_2 are usually in the range of 0.62–0.79 due to the various elemental compositions of marine plankton biomass. Zhai et al. (2005) and Wang et al. (2015) supposed that estuarine organic carbon may include more reduced molecules than the typical average OM. Therefore, the upper limit of ΔCO_2:ΔDO is 0.90, and the lower limit is 0.62. When ΔCO_2:ΔDO ≥ 1.0, the production of CO_2 exceeds that found when OM is fully mineralized under saturated oxygen conditions. This phenomenon is mainly attributed to the erosion of carbonate rocks by H^+. When ΔCO_2:ΔDO < 0.62, the consumption of DO does not produce the corresponding CO_2. Therefore, aerobic degradation of OM is not the main process controlling ΔCO_2:ΔDO. It is possible that the oxidation of reducing components such as Fe^{2+} in the river consumes most of the DO or that the anaerobic oxidation of OM produces organic acids rather than CO_2 (Zhai et al., 2005; Chen et al., 1996; Hedges et al., 2002).

$$(CH_2O)_{106}(NH_3)_{16}H_3PO_4 + 138O_2 + 18HCO_3^- \rightarrow 124CO_2 + 140H_2O + 16NO_3^- + HPO_4^{2-} \tag{11}$$

As can be seen from Fig. 5, the ratio of ΔCO_2:ΔDO followed a clear seasonal variation. During the rainy seasons of summer and autumn, the river water pH was relatively low. The dynamic transformation of DIC induced a greater proportion of $H_2CO_3^*$. Thus, the ΔCO_2 was greater in summer and autumn than in winter and spring. Commonly, biogeochemical processes are more robust in summer and autumn. The ratio of CO_2 loss to O_2 production during photosynthesis is about 0.97 (Zhai et al., 2005; Eq. (12)). Obviously, Fig. 5 does not reflect the signal of photosynthesis. The data points between 0.62 and 0.90 reflect the degradation of OM in summer and autumn.

$$67Ca^{2+} + 134HCO_3^- + 39CO_2 + 18H^+ + 16NO_3^- + HPO_4^{2-} + 122H_2O \rightarrow (CH_2O)_{106}(NH_3)_{16}(H_3PO_4) + 67CaCO_3 + 138O_2 \tag{12}$$

Most of the data points in winter and spring fell below 0.62, indicating that the consumption of DO did not produce a corresponding amount of excess CO_2. A high DO deficit makes it difficult for OM to be completely oxidized to CO_2. Its degradation products may be a series of small molecular organic compounds, such as organic acids (Richey et al., 1988; Salomão et al., 2008). Therefore, a systematic study of the sources and transport processes of DOC in the watershed became necessary. The data points of $\Delta CO_2 < 0$ indicate that the river water absorbed CO_2 from the atmosphere in winter and spring. Possible reasons include the precipitation of calcite and denitrification. These processes will increase the pH, then drive the dynamic transformation of DIC components to promote CO_2 deficit. Notably, AMD contains a large amount of reducing components, such as Fe^{2+}, and the oxidation of these ions consumes a large amount of DO without producing CO_2 (Atekwana and Fonyuy, 2009). The data points of ΔCO_2:ΔDO > 1.0 indicate that the excess CO_2 may have been due to the dynamic conversion of HCO_3^- to $H_2CO_3^*$ at low pH (Lee et al., 2021).

5.2.2. Co-evolution of DIC and alkalinity

The variation of alkalinity and DIC can reflect the carbon transport and transformation processes in surface water bodies. In weakly alkaline water, these two parameters usually show the law of co-evolution. Drawing on the idea of Jiang et al. (2013), HT1 at the head of the Huatan River was selected

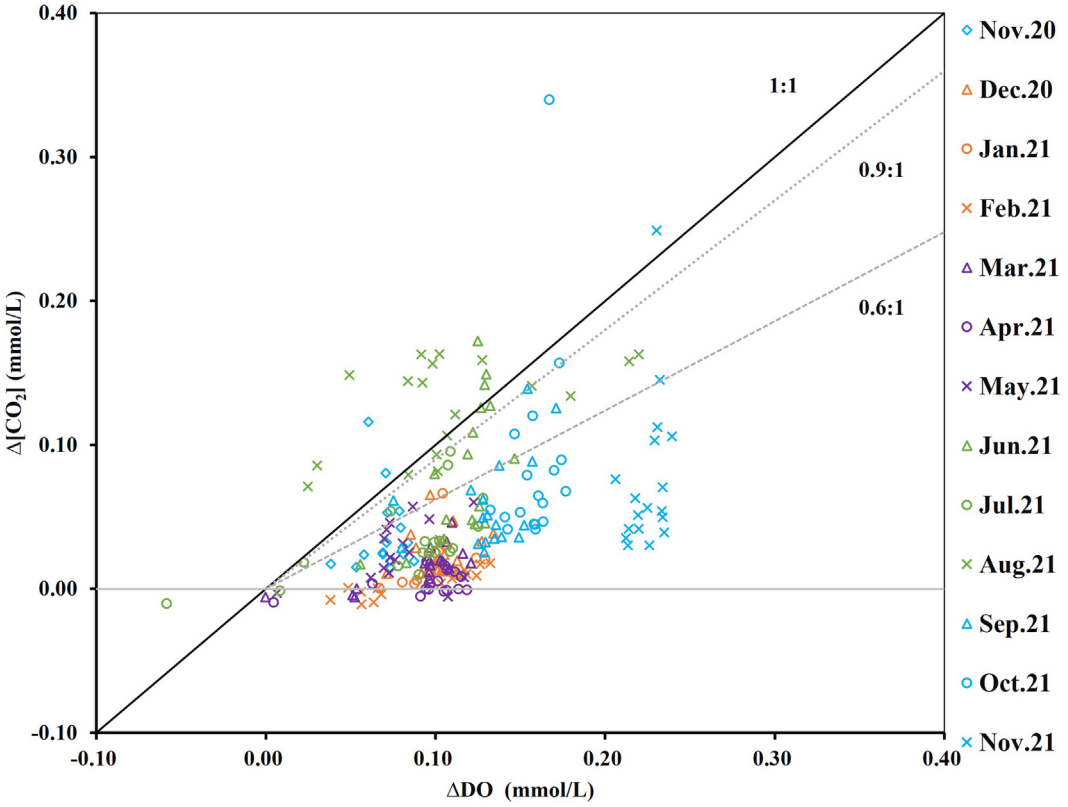

Fig. 5. Relationship between $\Delta[CO_2]$ and ΔDO in the Huatan River Basin.

as a reference to assess the evolutionary characteristics of DIC and alkalinity in the Huatan River, especially the CO_2 transport at the water-gas interface.

$$\Delta DIC = DIC_i - \frac{S_i}{S_1} \times DIC_1 \quad (13)$$

$$\Delta TA = TA_i - \frac{S_i}{S_1} \times TA_1 \quad (14)$$

In these equations, ΔDIC denotes the surplus or deficit of DIC at any sampling point, while ΔTA similarly indicates changes in alkalinity; S_i (S_1), DIC_i (DIC_1), TA_i (TA_1) represent the salinity, DIC concentration, and alkalinity at point i, respectively.

It is generally believed that, during the dissolution and precipitation of calcium carbonate, ΔTA and ΔDIC evolve along a 2:1 slope, as shown in Fig. 6 (Cai et al., 2004; Liu et al., 2014; Jiang et al., 2008). Although the transport of CO_2 at the water-gas interface does not affect TA, the concentration of DIC changes. On the X-axis of Fig. 6, the horizontal arrow to the left indicates CO_2 degassing, and the horizontal arrow to the right indicates the absorption of atmospheric CO_2. In these processes, DIC concentration varies, but TA remains stable. Under the influence of primary processes of productivity, such as photosynthesis and respiration, the ratio between ΔTA and ΔDIC is approximately 106:15 (Redfield et al., 1963). In domestic wastewater, DIC and TA are maintained at a high level; specifically, ΔTA:ΔDIC is approximately 0.97 (Li et al., 2017).

As shown in Fig. 6, DIC and TA in the Huatan River co-evolved mainly in accord with the ratio of ΔTA:ΔDIC = 1:1. The data points in the first quadrant show that terrestrial and domestic sewage inputs were the main reason for the increases in alkalinity and DIC (Herath et al., 2022). The contribution of the dissolution of carbonates and the respiration of the aquatic ecosystem was very limited. On the one hand, there are many villages along the Huatan River. The direct discharge of domestic sewage may be a main source of DIC. On the other hand, the vegetation coverage in the basin is high; thus, the mineralization of leaf litter is also likely to contribute large quantities of DIC.

In the third quadrant, the data points basically fall between geochemical processes such as CO_2 degassing, calcite precipitation, and photosynthesis. According to the calcite saturation index, the Huatan River showed the supersaturation of calcium carbonate in spring, and the precipitation of

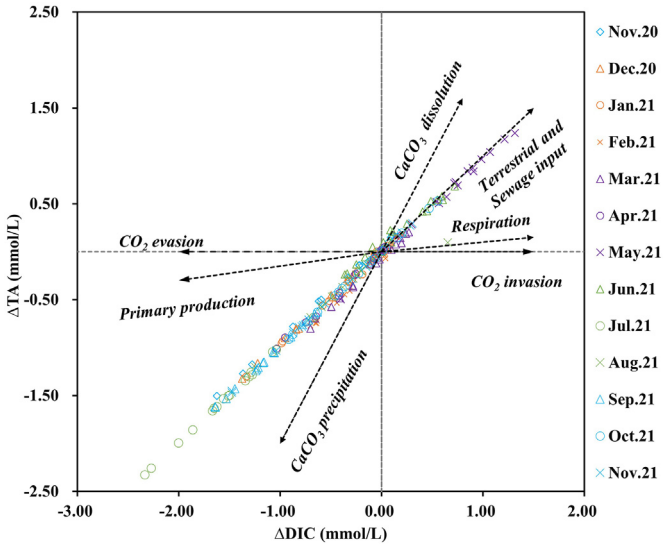

Fig. 6. Relationship between ΔTA and ΔDIC in the Huatan River Basin. ΔTA and ΔDIC were proportional, and the sampling points fell mainly in quadrants one and three, with quadrant one being influenced mainly by $CaCO_3$ dissolution, terrestrial and sewage inputs, and respiration. The third quadrant is mainly influenced mainly by primary production and $CaCO_3$ precipitation. In line ΔTA = 0, ΔDIC<0 shows the CO_2 degassing process and ΔDIC>0 shows the CO_2 invasion process.

calcite during this period caused the loss of DIC and TA. According to Fig. 5, OM degradation had a certain regulatory effect on DO and CO_2 in summer and autumn, but the impact of photosynthesis was relatively limited. However, OM degradation was also not the main factor controlling the co-evolution of TA and DIC (Fig. 6). Therefore, the CO_2 degassing is likely to be another significant factor affecting the co-evolution of TA and DIC in addition to calcite precipitation. The analysis of the buffering capacity appears to confirm that pH > 8.46 indicates the uptake of atmospheric CO_2, while when the pH was <8.46, the dissolved CO_2 in the waters gradually increased (Fig. 3). Thus, the data points in the third quadrant evolve along a 1:1 slope under the combined influence of CO_2 degassing and calcite precipitation.

There are various sources of organic matter in the Huatan River Basin. Due to the large number of towns and villages, the first important source is the domestic sewage discharged by nearby residents. The study area has high vegetation coverage, and a second important source is the mineralization of plant litter. The coal bearing strata in the study area are very developed, and the leaching of sedimentary OM in the process of mining development will also be an important source. The fourth one is mainly from aquatic ecosystems, such as the remains of phytoplankton. ΔTA/ΔDIC suggests obvious seasonal changes. In spring and summer, the mineralization of terrestrial OM and the input of domestic sewage contributed a certain amount of alkalinity and DIC to the Huatan River. In autumn and winter, affected by the precipitation of calcite and CO_2 degassing, this ratio showed a DIC and TA deficit.

5.2.3. Factors affecting DIC concentration and isotope changes

To gain a deeper understanding of the effects of such processes as the mineralization of OM from terrestrial and domestic sewage input, and carbonate rock dissolution on the evolution of DIC concentration and δ^{13}C-DIC in the Huatan River, we established the following method based on the relationship between ΔDIC2 concentration and $\Delta\delta^{13}$C-DIC (Alling et al., 2012; Yin et al., 2020; Fig. 7):

$$\Delta\left[\delta^{13}C_{DIC}\right] = \left[\delta^{13}C_{DIC}\right]_{(i)} - \left[\delta^{13}C_{DIC}\right]_{(1)} \quad (15)$$

$$\Delta[DIC] = [DIC]_{(i)} - [DIC]_{(1)} \quad (16)$$

Where Δ[DIC] and Δ[δ^{13}C-DIC] represent the DIC and δ^{13}C-DIC differences between any point and HT1 in the corresponding month, respectively.

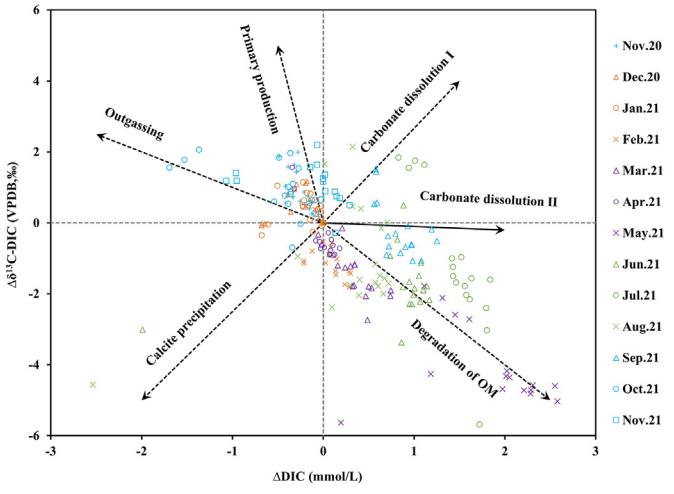

Fig. 7. Relationship between $\Delta\delta^{13}$C-DIC and ΔDIC in the Huatan River Basin. The four quadrants show the processes most likely to influence DIC, with the first quadrant mainly influenced by Carbonate dissolution I, the second quadrant by primary production and outgassing, the third quadrant by calcite precipitation, and the fourth quadrant by the degradation of OM and Carbonate dissolution II (CO_2 produced by organic matter degradation further dissolves carbonate rocks).

For samples collected in autumn and winter, most of the data points fall in the second quadrant, indicating that photosynthesis and CO_2 degassing may have been the two main factors for the decrease in DIC concentration and the heavier isotopic composition. Since the DIC concentration and isotope changes caused by the two processes were consistent, it is difficult to distinguish between the two processes (Samanta et al., 2015; Wang et al., 2019, 2020). However, according to the previous analysis, the influence of photosynthesis on the transport and transformation of DIC was limited (Fig. 6). Therefore, it can be concluded that the decrease in DIC concentration and the heavier isotopic composition were mainly caused by CO_2 outgassing.

The degradation of OM, respiration and the soil CO_2 influx tend to increase the content of DIC and lighten the carbon isotopic composition of DIC (Zhong et al., 2017; Zhong et al., 2018). Therefore, these processes would result in a negative correlation between ΔDIC and $\Delta\delta^{13}$C-DIC, as shown in Fig. 7 (De Montety et al., 2011; Alling et al., 2012; Wang et al., 2019, 2020). Due to the limited impact on DIC of aquatic ecological processes such as respiration, the data points in the fourth quadrant in Fig. 7 mainly revealed the degradation of OM. As mentioned in the previous analysis, there are many towns distributed along the Huatan River, and the input of domestic sewage is a major source of DIC. The degradation of a large amount of OM would have increased the content of DIC and lightened the δ^{13}C-DIC (Wachniew, 2006; Barnes and Raymond, 2009). Interestingly, carbonate dissolution pathway II displays a clear signal in Fig. 7. This path indicates that CO_2 produced by OM degradation was transformed into H_2CO_3, which then dissolved carbonate rocks. This process makes the isotopic composition of DIC reflect the mixed characteristics of carbon isotopic composition in OM and limestone.

5.3. The evolution of DIC in the Huatan River Basin

According to the above analysis, the factors affecting DIC transformation in the Huatan River include CO_2 degassing, the input of terrestrial and domestic sewage, OM degradation, $CaCO_3$ dissolution and precipitation, and AMD input. Based on the seasonal variations of hydrochemical composition, we developed a conceptual model to illustrate DIC transport and transformation in the Huatan River (Fig. 8).

In summer and autumn, the input of terrestrial and domestic sewage is a significant source of DIC, and the influence of photosynthesis on carbon transport is very limited. In summer, OM mineralization produces a large amount of CO_2 and further dissolves limestone in the form of H_2CO_3. Hence, the δ^{13}C-DIC reflects the superposition of the two sources (Romanek et al., 1992). In autumn, under the influence of AMD input, the oxidation of acid-producing metal ions makes the DO unsaturated, and CO_2 degassing makes the δ^{13}C-DIC heavier. Therefore, in summer and autumn, karstification is not the main process controlling DIC transmission and transformation. In other words, CO_2 degassing has a more significant influence on the evolution of DIC.

Winter and spring represent dry seasons for the Huatan River. The leaching of rainwater and the input of AMD are weakened. Correspondingly, the pH of the river water increases. During this period, the transport and transformation of DIC gradually weaken. In particular, the buffering capacity of water to carbonate components is the weakest in winter. DIC input reduces, and its concentration decreases gradually. Therefore, the CO_2 degassing gradually weakens, and the δ^{13}C-DIC reaches the heaviest level in winter. In spring, with rising temperatures, the OM degradation produces a large amount of CO_2, and DIC can be supplemented (Zhong et al., 2020). This process also leads to the precipitation of carbonate minerals. It can be seen that terrestrial and domestic sewage are still notable sources of DIC; moreover, karstification is not the main process affecting the transmission and transformation of DIC during this period.

6. Conclusion

(1) Controlled by the jointly influence of the weathering of carbonate rocks and sulfide-rich coal measures, river pH varied from 7.47 to 8.96 throughout the year, specifically, low in summer and autumn and

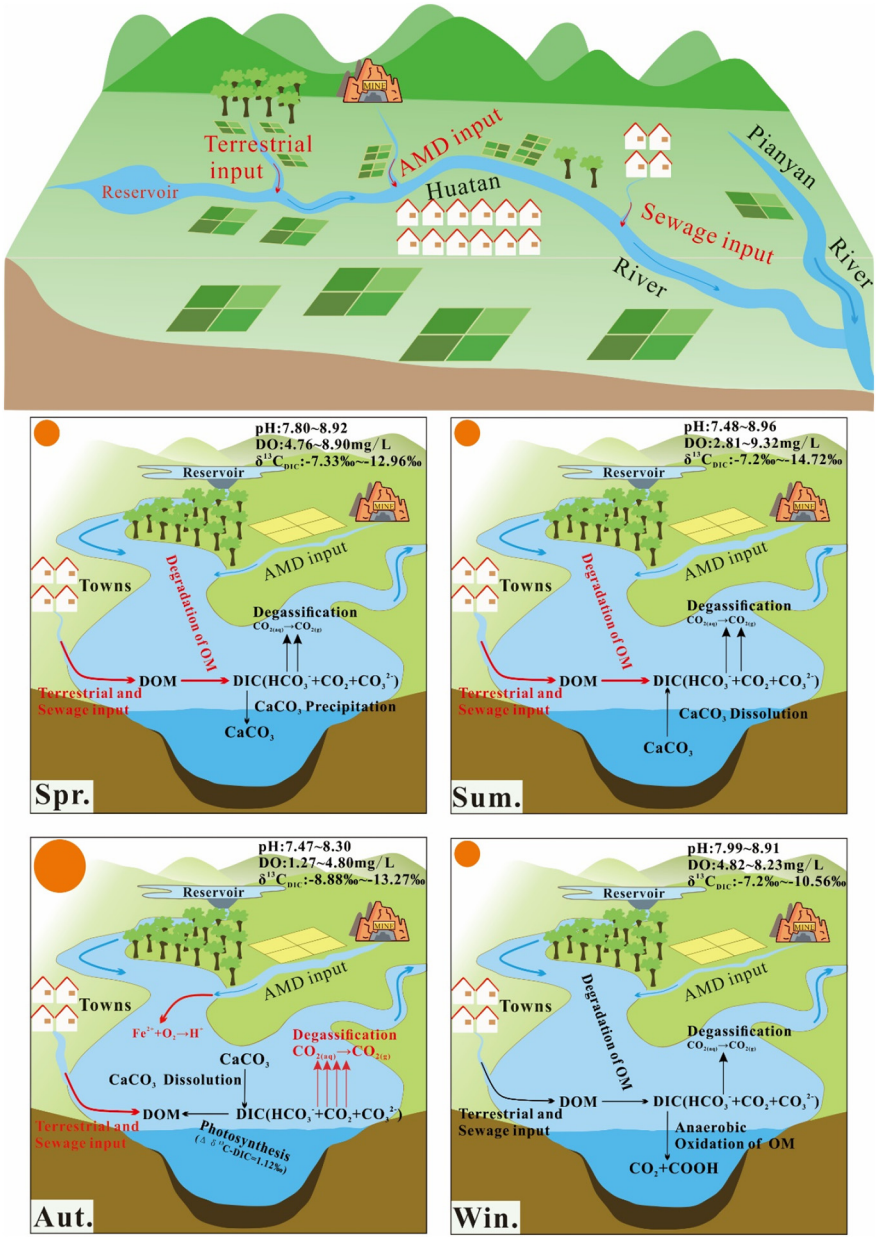

Fig. 8. Conceptual model of DIC evolution in the Huatan River Basin. The main processes affecting DIC evolution were degradation of OM; terrestrial and sewage input in spring and summer; photosynthesis and degassification in autumn; and the effects of various processes were weakened in winter.

high in winter and spring. The concentration of DIC ranged from 1.69 to 4.45 mmol/L, with an average of 3.45 mmol/L, which was high in summer and autumn and low in winter and spring. Seasonal variation was also evident in δ^{13}C-DIC, which was light in summer and autumn and heavy in winter and spring. Due to CO_2 degassing, DIC concentration spatially demonstrated a decreasing trend along the flow direction. Similarly, δ^{13}C-DIC was lighter upstream and heavier downstream.

(2) The buffering capacity to carbonate had obvious seasonal variation. In winter, the Revelle factor reached the maximum value, and the buffer capacity was the weakest. In spring, as pH increased, the concentration of CO_3^{2-} also increased, resulting in the oversaturation of $CaCO_3$. During this period, the buffer capacity related to CO_2 was enhanced. In summer and autumn, with the advent of the rainy season, the leaching of rainwater into the basin and the input of AMD increased, the pH decreased, and the Revelle factor decreased gradually, indicating that the dissolution capacity of carbonate rocks increased gradually.

(3) According to the results of our analysis of $\Delta[CO_2]$ and ΔDO stoichiometry, the co-evolution of DIC and alkalinity, and the correlation between $\Delta\delta^{13}$C-DIC and ΔDIC, the DIC transport and transformation in the Huatan River were influenced by the input of AMD, CO_2 degassing, the degradation of OM, $CaCO_3$ dissolution and precipitation, and so on. Starting from spring, the input of terrestrial and domestic sewage gradually enhanced and replenished DIC in the water. In summer, the OM degradation produced a large amount of CO_2, which then dissolved a certain amount of limestone. In autumn, the OM mineralization weakened, and CO_2 degassing was gradually increased under the influence of AMD input. In winter, CO_2 degassing gradually weakened, DIC concentration dropped to the lowest level of the year, and δ^{13}C-DIC reached its heaviest value of −7.2 ‰. The annual variation of δ^{13}C-DIC reaches 7.5 ‰ in the whole basin.

CRediT authorship contribution statement

Huang Jiangxun: Collected the data, Performed the analysis, Wrote the paper

Li Qingguang: Conceived and designed the analysis, Collected the data, Performed the analysis, Wrote the paper, Manuscript correction

Wu Pan: Conceived and designed the analysis, Performed the analysis

Wang Shilu: Performed the analysis, Manuscript correction

Liu Kun: Experimental tests

Guo Mingwei: Experimental tests

Declaration of competing interest

The authors declare that they have no known competing financial interests or personal relationships that could have appeared to influence the work reported in this paper.

Acknowledgements

This study was sponsored by the National Natural Science Foundation of China (Nos. 41867050, U1612442), the National Key Research and Development Plan of China (No.2019YFC1805300), Guizhou Provincial Science and Technology Foundation (No.[2019]1096), Guizhou Province Talent Base Project (No.RCJD2018-21), First-class Discipline Construction Project of Guizhou Province (No.GNYL [2017] 007).

Appendix A. Supplementary data

Supplementary data to this article can be found online at https://doi.org/10.1016/j.scitotenv.2022.156436.

References

Alling, V., Porcelli, D., Mörth, C.M., Anderson, L.G., Sanchez-Garcia, L., Gustafsson, Ö., Andersson, P.S., Humborg, C., 2012. Degradation of terrestrial organic carbon, primary production and out-gassing of CO2 in the laptev and east Siberian seas as inferred from δ13C values of DIC. Geochim. Cosmochim. Acta 95, 143–159. https://doi.org/10.1016/j.gca.2012.07.028.

Atekwana, E.A., Fonyuy, E.W., 2009. Dissolved inorganic carbon concentrations and stable carbon isotope ratios in streams polluted by variable amounts of acid mine drainage. J. Hydrol. 372, 136–148. https://doi.org/10.1016/j.jhydrol.2009.04.010.

Barnes, R.T., Raymond, P.A., 2009. The contribution of agricultural and urban activities to inorganic carbon fluxes within temperate watersheds. Chem. Geol. 266. https://doi.org/10.1016/j.chemgeo.2009.06.018.

Beaulieu, E., Goddéris, Y., Donnadieu, Y., Labat, D., Roelandt, C., 2012. High sensitivity of the continental-weathering carbon dioxide sink to future climate change.2. Nat. Clim. Chang. https://doi.org/10.1038/nclimate1419.

Broecker, W.S., Takahashi, T., Simpson, H.J., Peng, t, 1979. Fate of fossil fuel carbon dioxide and the global carbon budget. Science 206, 409–418. https://doi.org/10.1126/science.206.4417.409.

Cai, W.J., Dai, M.H., Wang, Y.C., Zhai, W.D., Huang, T., Chen, S.T., Zhang, F., Chen, Z.Z., Wang, Z.H., 2004. The biogeochemistry of inorganic carbon and nutrients in the Pearl River estuary and the adjacent northern South China Sea. Con. Shelf. Res. 24. https://doi.org/10.1016/j.csr.2004.04.005.

Chen, C.T.A., Lin, C.M., Huang, B.T., Chang, L.F., 1996. Stoichiometry of carbon, hydrogen, nitrogen, sulfur and oxygen in the particulate matter of the western North Pacific marginal seas. Mar. Chem. 54, 179–190. https://doi.org/10.1016/0304-4203(96)00021-7.

Chen, S., Zhong, J., Li, S.L., Ran, L.S., Wang, W.F., Xu, S., Yan, Z.L., Xu, S., 2021. Multiple controls on carbon dynamics in mixed karst and non-karst mountainous rivers, Southwest China, revealed by carbon isotopes (δ13C and Δ14C). Sci. Total Environ. 148347. https://doi.org/10.1016/j.scitotenv.2021.1.

Duvert, C., Bossa, M, Tyler, K.J., Wynn, J.G., Munksgaard, N.C., Bird, M.I., Setterfield, S.A., Hutley, L.H., 2019. Groundwater-derived DIC and carbonate buffering enhance fluvial CO_2 evasion in two Australian tropical Rivers. J. Geophys. Res. Biogeosci. 124, 312–327. https://doi.org/10.1029/2018JG004912.

Egleston, E.S., Sabine, C.L., Morel, F.M.M., 2010. Revelle revisited: buffer factors that quantify the response of ocean chemistry to changes in DIC and alkalinity. Glob. Biogeochem. Cycles 24. https://doi.org/10.1029/2008gb003407.

Elghali, A., Benzaazoua, M., Bouzahzah, H., Bussière, B., Villarraga-Gómez, H., 2018. Determination of the available acid-generating potential of waste rock, part I: mineralogical approach. Appl. Geochem. 99, 31–41. https://doi.org/10.1016/j.apgeochem.2018.10.021.

Fonyuy, E.W., Atekwana, E.A., 2008a. Dissolved inorganic carbon evolution and stable carbon isotope fractionation in acid mine drainage contaminated streams: insights from a laboratory study. Appl. Geochem. 23, 2634–2648. https://doi.org/10.1016/j.apgeochem.2008.05.012.

Fonyuy, E.W., Atekwana, E.A., 2008b. Effects of acid mine drainage on dissolved inorganic carbon and stable carbon isotopes in receiving streams. Appl. Geochem. 23, 743–764. https://doi.org/10.1016/j.apgeochem.2007.12.003.

Gombert, P., 2002. Role of karstic dissolution in global carbon cycle. Glob. Planet. Chang. 33, 177–184. https://doi.org/10.1016/S0921-8181(02)00069-3.

Han, G.L., Liu, C.Q., 2004. Water geochemistry controlled by carbonate dissolution: a study of the river waters draining karst-dominated terrain, Guizhou Province, China. Chem. Geol. 204, 1–21. https://doi.org/10.1016/j.chemgeo.2003.09.009.

Hauck, J., Völker, C., 2015. Rising atmospheric CO2 leads to large impact of biology on Southern Ocean CO2 uptake via changes of the revelle factor. Geophys. Res. Lett. 42, 1459–1464. https://doi.org/10.1002/2015GL063070.

Hedges, J.I., Baldock, J.A., Gélinas, Y., Lee, C., Peterson, M.L., Wakeham, S.G., 2002. The biochemical and elemental compositions of marine plankton: a NMR perspective. Mar. Chem. 78, 47–63. https://doi.org/10.1016/S0304-4203(02) 00009-9.

Herath, I.K., Wu, S.J., Ma, M.H., Huang, Ping, 2022. Dynamic of riverine pCO2, biogeochemical characteristics, and carbon sources inferred from δ13C in a subtropical river system. Sci. Total Environ. 821. https://doi.org/10.1016/J.SCITOTENV.2022.153296.

Jiang, L.Q., Cai, W.J., Wang, Y.C., 2008. A comparative study of carbon dioxide degassing in river and marine-dominated estuaries. Limnol. Oceanogr. 53, 2603–2615. https://doi.org/10.4319/lo.2008.53.6.2603.

Jiang, L.Q., Cai, W.J., Wang, Y., Bauer, J.E., 2013. Influence of terrestrial inputs on continental shelf carbon dioxide. Biogeosciences 10, 839–849. https://doi.org/10.5194/bg-10-839-2013.

Lee, K.Y., Van, G.R., Barth, J.A.C., 2021. Extreme gradients in CO2 losses downstream of karstic springs. Sci. Total Environ. 778, 146099–1496099. https://doi.org/10.1016/J.SCITOTENV.2021.146099.

Li, Y.X., Yang, X.F., Han, P., Xue, L., Zhang, L.J., 2017. Controlling mechanisms of surface partial pressure of CO2 in Jiaozhou Bay during summer and the influence of heavy rain. J. Mar. Syst. 173, 49–59. https://doi.org/10.1016/j.jmarsys.2017.04.006.

Liu, J.K., Han, G.L., 2020. Effects of chemical weathering and CO2 outgassing on δ13C-DIC signals in a karst watershed. J. Hydrol. 589. https://doi.org/10.1016/j.jhydrol.2020.125192.

Liu, Z., Zhao, J., 2000. Contribution of carbonate rock weathering to the atmospheric CO2 sink. Environ. Geol. 39, 1053–1058. https://doi.org/10.1007/s002549900072.

Liu, Z.H., Dreybrodt, W., Wang, H.J., 2010. A new direction in effective accounting for the atmospheric CO2 budget: considering the combined action of carbonate dissolution, the global water cycle and photosynthetic uptake of DIC by aquatic organisms. Earth Sci. Rev. 99, 162–172. https://doi.org/10.1016/j.earscirev.2010.03.001.

Liu, Z.Y., Zhang, L.J., Cai, W.J., Wang, L., Xue, M., Zhang, X.S., 2014. Removal of dissolved inorganic carbon in the Yellow River estuary. Limnol. Oceanogr. 59. https://doi.org/10.4319/lo.2014.59.2.0413.

Liu, Z.H., Macpherson, G.L., Groves, C., Jonathan, B.M., Yuan, D.X., Zeng, S.B., 2018. Large and active CO2 uptake by coupled carbonate weathering. Earth-Sci. Rev. 182, 42–49. https://doi.org/10.1016/j.earscirev.2018.05.007.

Lu, W.Q., Wang, S.L., Yeager, K.M., Liu, F., Huang, Q.S., Yang, Y.X., Xiang, P., Lü, Y.C., Liu, C.Q., 2018. Importance of considered organic versus inorganic source of carbon to lakes for calculating net effect on landscape C budgets. J. Geophys. Res. Biogeosci. 123. https://doi.org/10.1002/2017JG004159.

Mayo, A.L., Petersen, E.C., Kravits, C., 2000. Chemical evolution of coal mine drainage in a non-acid producing environment, Wasatch Plateau, Utah, USA. J. Hydrol. 236, 1–16. https://doi.org/10.1016/s0022-1694(00)00277-8.

Montety, V.D., Martin, J.B., Cohen, M.J., Foster, C., Kurz, M.J., 2011. Influence of diel biogeochemical cycles on carbonate equilibrium in a karst river. Chem. Geol. 283. https://doi.org/10.1016/j.chemgeo.2010.12.025.

Mook, W.G., Bommerson, J.C., Staverman, W.H., 1974. Carbon isotope fractionation between dissolved bicarbonate and gaseous carbon dioxide. Earth. Planet. Sci. Lett. 22, 169–176. https://doi.org/10.1016/0012-821X(74)90078-8.

Redfield, A.C., Ketchum, B.H., Richards, F.A., 1963. The influence of organisms on the composition of sea-water. In: Hill, M.N. (Ed.), In the Sea. Wiley-Interscience, New York, pp. 26–77.

Revelle, R., Suess, H.E., 1957. Carbon dioxide exchange between atmosphere and ocean and the question of an increase of atmospheric CO2 during the past decades. Tellus 9, 18–27. https://doi.org/10.1111/j.2153-3490.1957.tb01849.x.

Richey, J.E., Devol, A.H., Wofsy, S.C., Victoria, R., Riberio, M.N.G., 1988. Biogenic gases and the oxidation and reduction of carbon in Amazon River and floodplain waters: Amazon dissolved gases. Limnol. Oceanogr. 33. https://doi.org/10.4319/lo.1988.33.4.0551.

Romanek, C.S., Grossman, E.L., Morse, J.W., 1992. Carbon isotopic fractionation in synthetic aragonite and calcite: effects of temperature and precipitation rate. Geochim. Cosmochim. Acta 56, 419–430. https://doi.org/10.1016/0016-7037(92)90142-6.

Rosentreter, J.A., Eyre, B.D., 2020. Alkalinity and dissolved inorganic carbon exports from tropical and subtropical river catchments discharging to the Great Barrier Reef, Australia. Hydrol. Process. 4 (7), 1530–1544. https://doi.org/10.1002/hyp.13679.

Salomão, M.S.M.B., Cole, J.J., Clemente, C.A., Silva, D.M.L., de Camargo, P.B., Victoria, R.L., Martinelli, 2008. CO2 and O2 dynamics in human-impacted watersheds in the state of Sa˜o Paulo, Brazil. Biogeochemistry 88, 271–283. https://doi.org/10.1007/s10533-008-9210-y.

Samanta, S., Dalai, T.K., Pattanaik, J.K., Rai, S.K., Mazumdar, A., 2015. Dissolved inorganic carbon (DIC) and its δ13C in the ganga (Hooghly) river estuary, India: evidence of DIC generation via organic carbon degradation and carbonate dissolution. Geochim. Cosmochim. Acta 165, 226–248. https://doi.org/10.1016/j.gca.2015.05.040.

Singer, P.C., Stumm, W., 1970. Acidic mine drainage: the rate-determining step. Science 167, 1121–1123. https://doi.org/10.1126/science.167.3921.

Song, X.W., Lyu, S.D., Sun, K., Gao, Y., Wen, X.F., 2021. Flux and source of dissolved inorganic carbon in a headwater stream in a subtropical plantation catchment. J. Hydrol. 600, 126511. https://doi.org/10.1016/j.jhydrol.2021.126511.

Teemu, K., Marja, L.R., Marja, L., Lena, A., 2018. Comparison of static and mineralogical ARD prediction methods in the nordic environment. Environ. Monit. Assess. 190, 719. https://doi.org/10.1007/s10661-018-7096-2.

Wachniew, P., 2006. Isotopic composition of dissolved inorganic carbon in a large polluted river: the Vistula, Poland. Chem. Geol. 233, 293–308. https://doi.org/10.1016/j.chemgeo.2006.03.012.

Wang, W.Y., Li, Q.G., 2021. The buffering effect of chemical equilibrium of CaCO3-CO32–HCO3- on CO2 in freshwater carbonate lake—a case study from Baihua Lake, Guizhou. Carsologica. Sin. 40, 572–579. https://doi.org/10.11932/karst2021y05.

Wang, S.L., Yeager, K.M., Wan, G.J., Liu, C.Q., Wang, Y.C., Lü, Y.C., 2011. Carbon export and HCO3- fate in carbonate catchments: a case study in the karst plateau of southwestern China. Appl. Geochem. 27, 64–72. https://doi.org/10.1016/j.apgeochem.2011.09.003.

Wang, W.F., Li, S.L., Zhong, J., Maberly, S.C., Li, C., Wang, F.S., Xiao, H.Y., Liu, C.Q., 2020. Climatic and anthropogenic regulation of carbon transport and transformation in a karst river-reservoir system. Sci. Total. Environ., 707. https://doi.org/10.1016/j.scitotenv.2019.135628.

Wang, S.L., Yeager, K.M., Wan, G.J., Liu, C.Q., Liu, F., Lü, Y.C., 2015. Dynamics of CO2 in a karst catchment in the southwestern plateau, China. Environ. Earth Sci. 73, 2415–2427. https://doi.org/10.1007/s12665-014-3591-0.

Wang, W.F., Li, S.L., Zhong, J., Li, C., Yi, Y.B., Chen, S.N., Ren, Y.M., 2019. Understanding transport and transformation of dissolved inorganic carbon (DIC) in the reservoir system using δ13C-DIC and water chemistry. J. Hydrol. 574, 193–201. https://doi.org/10.1016/j.jhydrol.2019.04.036.

Weyhenmeyer, G.A., Kosten, S., Wallin, M.B., Tranvik, L.J., Jeppesen, E., Roland, F., 2015. Significant fraction of CO2 emissions from boreal lakes derived from hydrologic inorganic carbon inputs. Nat. Geosci. 8, 933–936. https://doi.org/10.1038/ngeo2582.

Yin, X.J., Lin, Y.P., Liang, C.C., Tao, S.Q., Wang, L., Xu, Y.H., Li, Y.H., 2020. Source and fate of dissolved inorganic carbon in Jiulong River, southeastern China. Estuar. Coast. Shelf Sci. 246, 107031. https://doi.org/10.1016/j.ecss.2020.107031.

Zhai, W.D., Dai, M.H., Cai, W.J., Wang, Y.C., Wang, Z.H., 2005. High partial pressure of CO2 and its maintaining mechanism in a subtropical estuary: the Pearl River estuary, China. Mar. Chem. 93, 21–32. https://doi.org/10.1016/j.marchem.2004.07.003.

Zhang, C.N., 1999. Study on calculation method saturation values of dissolved oxygen in waters. Res. Environ. Sci. 12, 57–58. https://doi.org/10.13198/j.res.1999.02.57.zhangchn.013.

Zhang, J., Quay, P.D., Wilbur, D.O., 1995. Carbon isotope fractionation during gas-water exchange and dissolution of CO2. Geochim. Cosmochim. Acta 59. https://doi.org/10.1016/0016-7037(95)91550-D.

Zhang, L.J., Xue, M., Wang, M., Cai, W.J., Wang, L., Yu, Z.G., 2014. The spatiotemporal distribution of dissolved inorganic and organic carbon in the main stem of the changjiang (Yangtze) river and the effect of the three gorges reservoir. J. Geophys. Res. Biogeosci. 119, 741–757. https://doi.org/10.1002/2012JG002230.

Zhang, T., Li, J.H., Pu, J.B., Yuan, D.X., 2019. Carbon dioxide exchanges and their controlling factors in Guijiang River, SW China. J. Hydrol. 578. https://doi.org/10.1016/j.jhydrol.2019.124073.

Zhong, J., Li, S.L., Tao, F.X., Yue, F.J., Liu, C.Q., 2017. Sensitivity of chemical weathering and dissolved carbon dynamics to hydrological conditions in a typical karst river. Sci. Rep.-UK 7. https://doi.org/10.1038/srep42944.

Zhong, J., Li, S.L., Liu, J., Ding, H., Sun, X.L., Xu, S., Wang, T.J., Ellam, R.M., Liu, C.Q., 2018. Climate variability controls on CO2 consumption fluxes and carbon dynamics for monsoonal rivers: evidence from Xijiang River, Southwest China. J. Geophys. Res. Biogeosci. https://doi.org/10.1029/2018jg004439.

Zhong, J., Li, S.L., Ibarra, D.E., Ding, H., Liu, C.Q., 2020. Solute production and transport processes in Chinese monsoonal Rivers: implications for global climate change. Glob. Biogeochem. Cycles 34. https://doi.org/10.1029/2020gb006541.

Zhong, J., Wallin, M.B., Wang, W.F., Li, S.L., Guo, L.D., Dong, K.J., Ellam, R.M., Liu, C.Q., Xu, S., 2021. Synchronous evaporation and aquatic primary production in tropical river networks. Water Res. 200, 117272. https://doi.org/10.1016/j.watres.2021.1172.